Journal of Alloys and Compounds 509 (2011) 5672–5676

Contents lists available at ScienceDirect

Journal of Alloys and Compounds

journal homepage: www.elsevier.com/locate/jallcom

Hydrothermal synthesis of $MnCO_3$ nanorods and their thermal transformation into Mn_2O_3 and Mn_3O_4 nanorods with single crystalline structure

Xiaoping Shen [a,*], Zhenyuan Ji [a], Huajuan Miao [a], Juan Yang [b], Kangmin Chen [b]

[a] School of Chemistry and Chemical Engineering, Jiangsu University, Zhenjiang 212013, China
[b] School of Materials Science and Engineering, Jiangsu University, Zhenjiang 212013, China

ARTICLE INFO

Article history:
Received 4 August 2010
Received in revised form 20 February 2011
Accepted 22 February 2011
Available online 1 March 2011

Keywords:
Nanorods
Manganese oxide
Manganese carbonate
Synthesis
Lithium ion batteries

ABSTRACT

$MnCO_3$ nanorods with diameters of 50–150 nm and lengths of about 1–2 μm have been prepared for the first time by a facile hydrothermal method. Mn_2O_3 and Mn_3O_4 nanorods were obtained via the heat-treatment of the $MnCO_3$ nanorods in air and nitrogen atmosphere, respectively. The morphology and structure of the as-synthesized $MnCO_3$, Mn_2O_3 and Mn_3O_4 nanorods were characterized by X-ray diffraction, scanning electron microscopy, transmission electron microscopy and selected area electron diffraction. It was found that the $MnCO_3$ nanorods are single-crystalline, and their morphology and single-crystalline characteristic can be sustained after thermal transformation into Mn_2O_3 and Mn_3O_4. The corresponding growth directions for $MnCO_3$, Mn_2O_3 and Mn_3O_4 nanorods were [2 1 4], [1 0 0] and [1 1 2], respectively. When applied as anode materials for lithium ion batteries, the Mn_2O_3 and Mn_3O_4 nanorods exhibited a reversible lithium storage capacity of 998 and 1050 mAh/g, respectively, in the first cycles.

1. Introduction

One-dimensional (1D) nanostructures such as nanorods, nanowires, nanotubes and nanobelts have aroused continuous interest among materials scientists for their crucial role in future technological advances in electronics, optoelectronics, and memory devices [1–3]. Up to now, a large number of 1D nanostructures with a wide variety of substances have been successfully synthesized with various methods including microemulsion, hydrothermal, sol–gel, chemical vapor deposition and template methods, etc. [4–7]. Manganese oxide materials have been extensively investigated due to their wide-spread applications in catalysts, molecular sieves, secondary batteries, ion exchange and magnetic materials [8–12]. Among them, polymorphs of Mn_2O_3 have proven to be inexpensive, environment-friendly catalysts for oxidation of organic pollutants and decomposition of nitrogen oxide [13,14]. In addition, Mn_2O_3 can also be used as an inexpensive precursor for the preparation of soft magnetic materials such as manganese zinc ferrite [15]. Mn_3O_4 is well known to be a good candidate as an active catalyst in various oxidation and reduction reaction. It can be used to limit the emission of NO_x and CO, which provides a powerful method of controlling air pollution [16]. Moreover, Mn_3O_4 was reported to be a promising material in electrochromic application [17]. Considering above application potentials, many studies have been done to develop various methods for the synthesis of Mn_2O_3 and Mn_3O_4 nanoparticles. Among the various methods developed, thermal decomposition is a rapid and effective approach to Mn_2O_3 and Mn_3O_4 nanoparticles [18]. $MnCO_3$ has been demonstrated to be an important precursor for the synthesis of manganese oxides through high-temperature calcination process [19–23]. However, to the best of our knowledge, the synthesis of $MnCO_3$ nanorods and their transformation into Mn_2O_3 and Mn_3O_4 nanorods are not reported so far.

Rechargeable lithium ion batteries have attracted worldwide research interest because of their high energy density and design flexibility [10]. Although Mn_2O_3 and Mn_3O_4 nanoparticles have been used as starting materials in the preparation of Li–Mn–O electrode materials for rechargeable lithium ion batteries [24–27], the electrochemical performance of Mn_2O_3 and Mn_3O_4 nanorods as the anode materials for lithium ion batteries were rarely studied. Herein, we report a facile hydrothermal method for the large-scale synthesis of $MnCO_3$ nanorods and their transformation into Mn_2O_3 and Mn_3O_4 nanorods by controlling the calcination processes. The electrochemical performances of the as-prepared Mn_2O_3 and Mn_3O_4 nanorods as anode materials of lithium ion batteries were also investigated.

2. Experimental

2.1. Preparation of $MnCO_3$ nanorods

All of the chemical reagents used in our experiments were of analytical grade, purchased from Shanghai Chemical Reagent Company, and used without further

* Corresponding author. Tel.: +86 511 88791800; fax: +86 511 88791800.
E-mail address: xiaopingshen@163.com (X. Shen).

0925-8388/$ – see front matter © 2011 Elsevier B.V. All rights reserved.
doi:10.1016/j.jallcom.2011.02.119

purification. In a typical procedure, 0.1 g of PVP (K-30; M_w = 40,000), 0.08 g of $KMnO_4$ and 0.396 g of $MnCl_2{\cdot}4H_2O$ were dissolved in 15 ml distilled water and then 0.5 ml of H_2O_2 was added dropwise. After stirring for 30 min, 10 ml of Li_2CO_3 (0.084 g) aqueous solution was added into the mixed solution. The resulting mixture was transferred into a 30 ml Teflon-lined stainless steel autoclave and heated at 180 °C for 24 h. The as-synthesized solid products were separated by centrifugation, washed thoroughly with water and absolute ethanol to remove any impurities, and then dried in vacuum oven at 60 °C for 12 h.

2.2. Preparation of Mn_2O_3 and Mn_3O_4 nanorods

Mn_2O_3 and Mn_3O_4 nanorods were prepared by thermal decomposition of the pre-formed $MnCO_3$ nanorods at different conditions. In a typical experiment for the preparation of Mn_2O_3 nanorods, the $MnCO_3$ nanorods were heated to 500 °C with a heating rate of 5 °C min^{-1} and kept at 500 °C for 3 h in air atmosphere, then naturally cooled to room temperature. For Mn_3O_4 nanorods, they were prepared in a way similar to that of Mn_2O_3 nanorods, except for the use of nitrogen instead of air as reaction atmosphere.

2.3. Instrumentation and measurements

The phase of as-synthesized products were characterized using X-ray diffraction (XRD, Shimadzu XRD-6000) with Cu Kα radiation (λ = 1.5406) at a scanning rate of 4° min^{-1}. X-ray tubes were operated with electric current of 30 mA and voltage of 40 kV. The composition, morphology, and size of the products were examined by field emission scanning electron microscopy (FESEM; JSM-7001), energy dispersive X-ray spectroscopy (EDS, attached to FESEM), and transmission electron microscopy (TEM; JEOL-2100). Samples for TEM were prepared by dropping the products on a carbon-coated copper grid after ultrasonic dispersing in absolute ethanol and allowed them to dry in air before analysis.

2.4. Electrochemical characterizations

Active materials (Mn_2O_3 or Mn_3O_4 nanorods) were mixed with acetylene black and poly(vinylidene fluoride) (PVdF), at weight ratios of 70:20:10 in *N*-methyl-2-pyrrolidone (NMP) solvent to form a slurry. The electrodes were formed by coating the slurry onto Cu foils and pressed under a pressure of approximately 200 kg/cm^2 after dried at 120 °C in a vacuum oven for 12 h. The cell assembly was operated in a glovebox filled with pure argon (99.999%) in the presence of an oxygen scavenger and a sodium-drying agent. The electrolyte was 1 M $LiPF_6$ in a 1:1 mixture of ethylene carbonate and dimethyl carbonate. Li metal foil was used as the counter and reference electrode. The electrode capacity was measured by a galvanostatic discharge/charge method at a current density of 0.1 C within the range 0.01 V to 3.0 V.

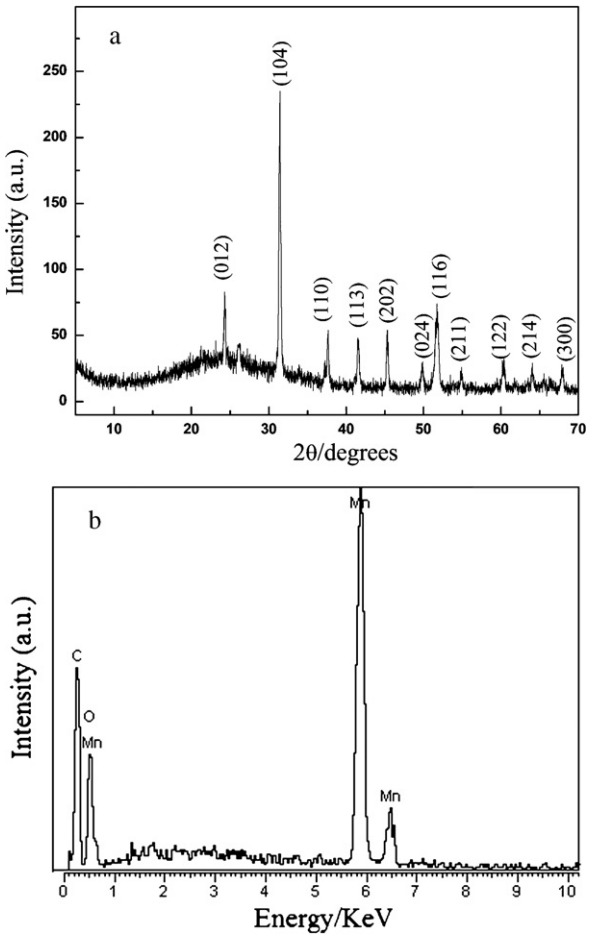

Fig. 1. (a) XRD pattern and (b) EDS spectrum of the as-prepared $MnCO_3$ nanorods.

3. Results and discussion

3.1. Characterization of the $MnCO_3$ nanorods

The XRD pattern of manganese carbonate prepared by hydrothermal reduction method is shown in Fig. 1a. All of the diffraction peaks can be easily indexed to a single phase of rhombohedral structure $MnCO_3$ with lattice constants a = 4.778 Å and c = 15.721 Å, which are slightly larger than the standard values for bulk rhombohedral $MnCO_3$ (JCPDS No. 86-0173, a = 4.772 Å and c = 15.637 Å). The energy-dispersive spectroscopy (EDS) (Fig. 1b) confirms that the nanorods are composed of carbon, manganese, and oxygen elements and no other impurity elements were detected, indicating the high purity of the final product.

The morphology and size of the as-prepared $MnCO_3$ sample were studied by FESEM. Fig. 2a and b shows the FESEM images of the products at different magnification, From Fig. 2a, it can be clearly seen that all the products have a rod-like morphology. More careful examination by the high-magnification FESEM image (Fig. 2b) reveals that the $MnCO_3$ nanorods are very smooth and straight, and their diameter and length are about 50–150 nm and 1–2 μm, respectively. A further investigation on the $MnCO_3$ nanorods was conducted by TEM and high-resolution TEM analyses. Fig. 2c shows the TEM image of the $MnCO_3$ nanorods, which further demonstrates that every nanorod is straight and has a uniform diameter along its whole length. These nanorods have a diameter of about 50–150 nm and a length of about 1–2 μm, which are consistent with the FESEM observation. A typical selective area electron diffraction (SAED) pattern (insert in Fig. 2d) taken from an individual nanorod with a diameter of about 100 nm (Fig. 2d) shows regular diffraction spots, which can be indexed to the rhombohedral $MnCO_3$ recorded from the [−4–21] zone axis and demonstrates that the $MnCO_3$ nanorod is single-crystalline and grows along the [2 1 4] direction.

Although the actual process involved in the synthesis of $MnCO_3$ nanorods may be quite complex, the in situ reaction can be briefly expressed as follows:

$$2MnO_4^- + 8Mn^{2+} + 5H_2O_2 + 10CO_3^{2-} \rightarrow 10MnCO_3\downarrow + 5O_2\uparrow + 6OH^- + 2H_2O$$

When using Na_2CO_3 or K_2CO_3 instead of Li_2CO_3 as the starting material in the synthesis, the obtained products only contain a small amount of rod-like architectures. This suggests that lithium ions play an important role in the formation of the $MnCO_3$ nanorods. Although the details of the effect of lithium ions on the formation of $MnCO_3$ nanorods is not clear up to date, it is well known that the anisotropic growth of nanoparticles can be achieved by the specific adsorption of ions to particular crystal surface, therefore, inhibiting the growth of these faces by lowering their surface energy. As reported in the literatures [28,29], the different radius of the cations of Li^+, Na^+ and K^+ can induce different interactions between these cations and WO_3 nanocrystals, which led to different morphologies of WO_3 products. It is reasonable to suppose that a similar situation also occurred in our present work, though a more in-depth study is necessary to further understand the growth process of $MnCO_3$ nanorods.

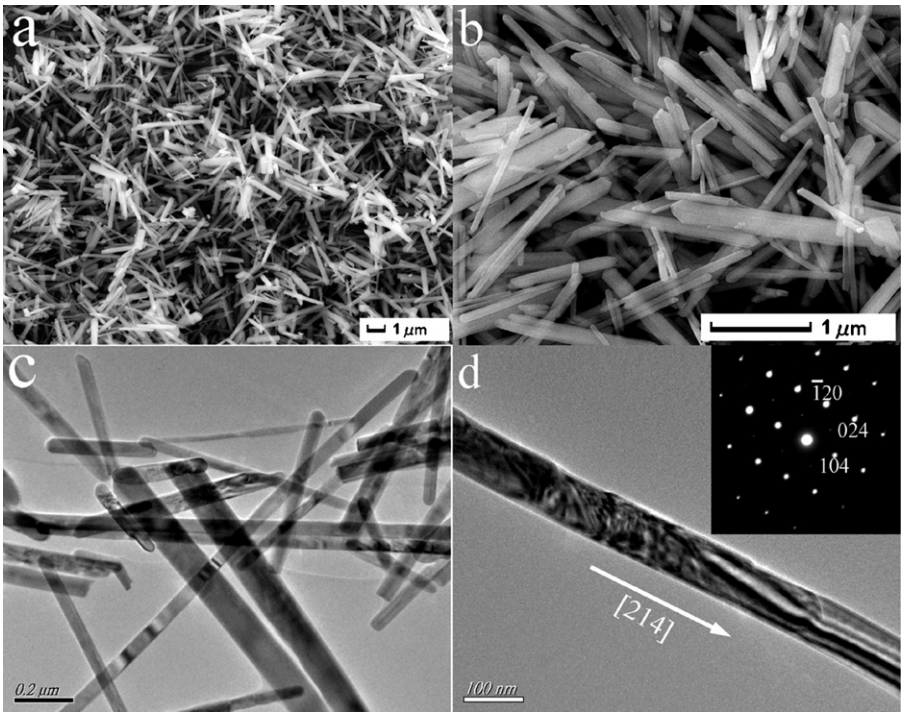

Fig. 2. (a, b) FESEM images and (c, d) TEM images of the $MnCO_3$ nanorods. The inset in 2d is the corresponding SAED pattern.

3.2. Characterization of the Mn_2O_3 and Mn_3O_4 nanorods

To investigate the effect of annealing condition on the products of $MnCO_3$ decomposition, the $MnCO_3$ precursor was annealed under different atmosphere: air and nitrogen. As a result, two manganese oxides with different manganese oxidation states were obtained. Annealing of the $MnCO_3$ nanorods in air at 500 °C for 3 h led to the formation of pure Mn_2O_3, which is consistent with those reported by the literatures [28,29]. In contrast, annealing in nitrogen atmosphere at 500 °C for 3 h led to the formation of pure Mn_3O_4, in which the temperature (500 °C) is much lower than that (900 °C) needed to convert $MnCO_3$ to Mn_3O_4 in air [30,31].

Fig. 3 shows the XRD patterns of the Mn_2O_3 and Mn_3O_4 nanorods obtained from heat-treatment of the $MnCO_3$ nanorods in air and nitrogen atmosphere, respectively. All the diffraction peaks of the product obtained in air atmosphere (Fig. 3a) can be indexed to cubic Mn_2O_3 with lattice constants of $a = 9.409$ Å, which

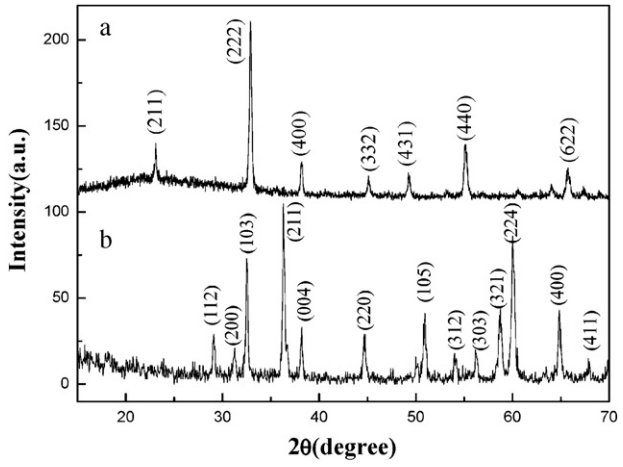

Fig. 3. XRD patterns of the as-synthesized (a) Mn_2O_3 and (b) Mn_3O_4 nanorods.

are well consistent with the values reported for bulk cubic Mn_2O_3 (JCPDS No. 41-1442). No other phases were observed in the products, indicating the complete transformation of $MnCO_3$ into Mn_2O_3. Fig. 3b shows the XRD patterns of the Mn_3O_4 nanorods, where all of the diffraction peaks can be easily indexed to tetragonal phase Mn_3O_4 with lattice constants $a = 5.7215$ Å and $c = 9.4081$ Å, which are slightly smaller than the standard values for bulk tetragonal Mn_3O_4 (JCPDS No. 24-0734, $a = 5.7621$ Å and $c = 9.4694$ Å).

The micromorphology of the Mn_2O_3 and Mn_3O_4 products were examined by FESEM and TEM. As shown in Fig. 4a and b, FESEM images reveal that both the Mn_2O_3 and Mn_3O_4 samples are composed of a large number of nanorods. The TEM micrographs (Fig. 4c and d) show that the Mn_2O_3 and Mn_3O_4 nanorods have a diameter of about 50–150 nm, which is consistent with that of $MnCO_3$ nanorods precursor. Therefore, the morphology and size of the $MnCO_3$ nanorods are well retained after thermal transformation into Mn_2O_3 and Mn_3O_4. The structural orientations of individual nanorods were also investigated. Fig. 4e shows a TEM image of a single Mn_2O_3 nanorod with a diameter of about 80 nm, and the corresponding SAED pattern (inset in Fig. 4e) with regular diffraction spots can be indexed to the cubic Mn_2O_3 single-crystalline recorded from the [01–2] zone axis, demonstrating that the Mn_2O_3 nanorod grows along the [1 0 0] direction. Fig. 4g shows a HRTEM image of the Mn_2O_3 nanorod, from which the (2 1 1) lattice planes with a d-spacing of 0.38 nm can be clearly distinguished. It was found that the preferential growth direction inclined to the (2 1 1) lattice plane at an angle of 55°, which is in consistent with the [1 0 0] growth direction determined by SAED. Fig. 4f shows the TEM image of a single Mn_3O_4 nanorod with a diameter of about 120 nm, and the inset in Fig. 4f shows the corresponding SAED pattern, which can be indexed to the tetragonal phase Mn_3O_4 recorded from the [3–51] zone axis and demonstrates that the Mn_3O_4 nanorod is single crystal with a [1 1 2] growth direction. Fig. 4 h is a HRTEM image of the Mn_3O_4 nanorod, in which the interplanar spacing of 0.249 nm is coincident with that of (2 1 1) plane of tetragonal Mn_3O_4, further confirming the single-crystalline nature of the Mn_3O_4 nanorods.

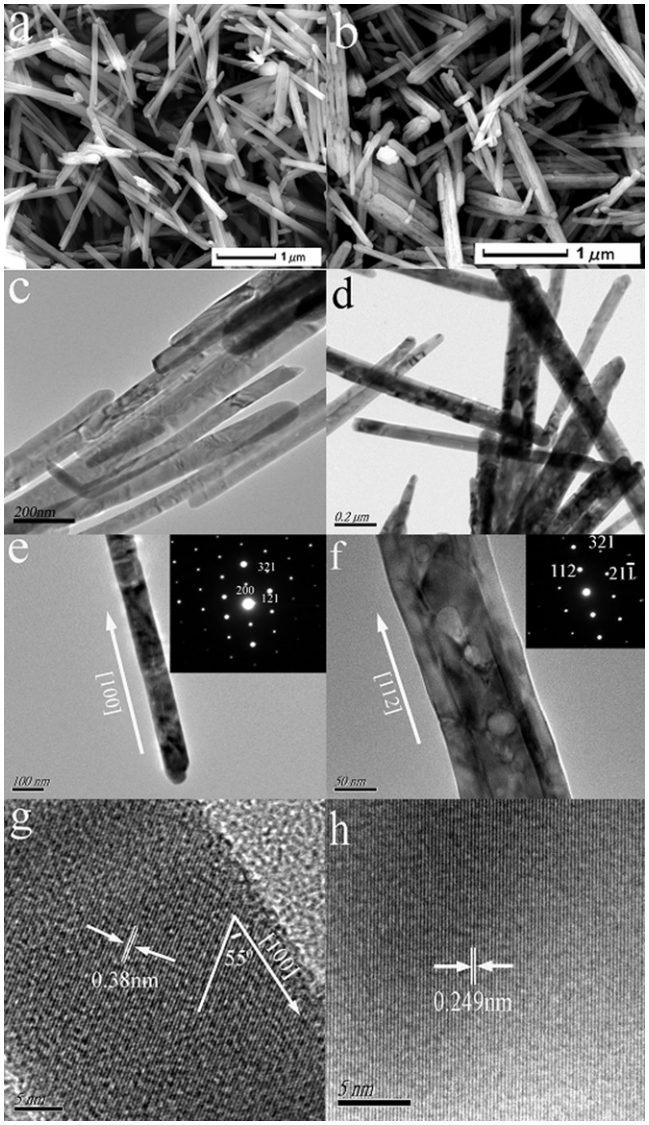

Fig. 4. SEM micrographs of the Mn_2O_3 (a) and Mn_3O_4 (b) nanorods. TEM images of the Mn_2O_3 (c, e) and Mn_3O_4 (d, f) nanorods, the insets in (e) and (f) are the corresponding SAED patterns. HRTEM images of the Mn_2O_3 (g) and Mn_3O_4 (h) nanorods.

3.3. Electrochemical performance of Mn_2O_3 and Mn_3O_4 nanorods

In this work, we also investigated the electrochemical performance of Mn_2O_3 and Mn_3O_4 nanorods as the anode materials for lithium ion batteries. The lithium storage capacity and cyclability were determined via galvanostatic charge/discharge cycling at a current density of 0.1 C. Fig. 5 displays the charge/discharge profiles of the Mn_2O_3 and Mn_3O_4 nanorods in the first cycle. The electrodes of Mn_2O_3 (Fig. 5a) and Mn_3O_4 (Fig. 5b) nanorods delivered a specific capacity of 998 and 1050 mAh/g in the initial discharging and a reversible capacity of 349 and 555 mAh/g in the first charging, respectively. The intercalation process of Li^+ and the structural evolution of Mn_2O_3 and Mn_3O_4 can be described as follows [32]:

$$3Mn_2O_3 + 2Li^+ + 2e^- \rightarrow 2Mn_3O_4 + Li_2O \quad (1)$$

$$Mn_3O_4 + Li^+ + e^- \rightarrow LiMn_3O_4 \quad (2)$$

$$LiMn_3O_4 + Li + + e^- \rightarrow 3MnO + Li_2O \quad (3)$$

$$MnO + 2Li^+ + 2e^- \leftrightarrow Mn + Li_2O \quad (4)$$

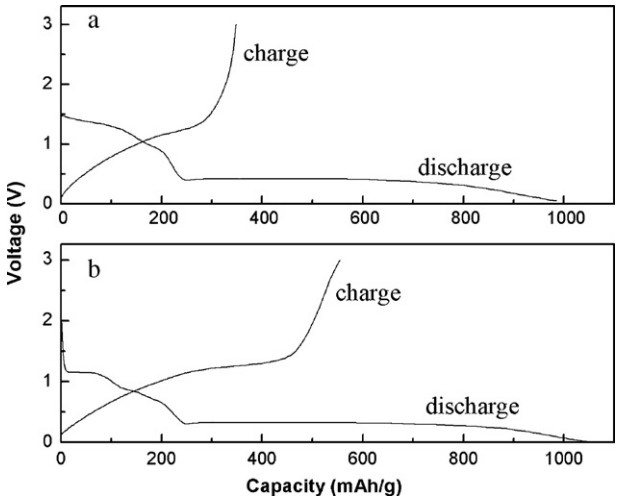

Fig. 5. The first discharge/charge profiles of the Mn_2O_3 (a) and Mn_3O_4 (b) nanorods electrodes at a current density of 0.1 C.

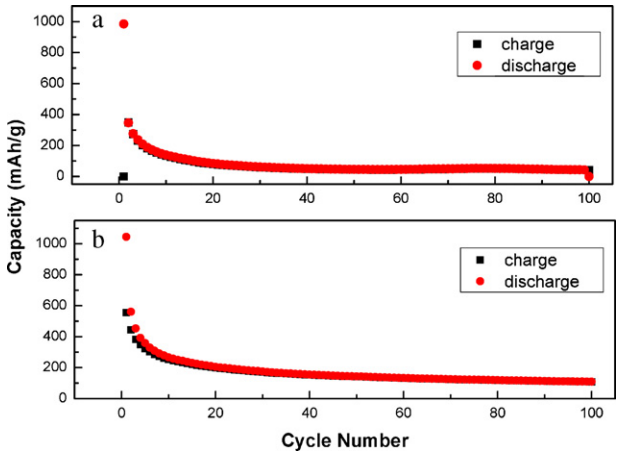

Fig. 6. Reversible lithium storage capacity *vs* cycle number for lithium ion batteries using the Mn_2O_3 (a) and Mn_3O_4 (b) nanorods as the anode electrode materials.

Therefore, Mn_2O_3 and Mn_3O_4 experience a similar phase transition pathway in the initial reduction process. Metallic Mn and Li_2O are the end products of discharge, while MnO is the end product of recharge for these two oxides [32]. This reaction mechanism is also supported by the significant capacity loss in the initial cycle. The cycling behaviors of the Mn_2O_3 and Mn_3O_4 nanorod electrodes are shown in Fig. 6. The Mn_2O_3 nanorod electrode (Fig. 6a) showed a rapid capacity loss with the increase of the cycle numbers and the capacity decreased to 50 mAh/g at the 40th cycle. After that, the capacity was almost maintained until the 96th cycle. The reason of such a phenomenon is not clear and remains to be further studied. Similarly, the discharge capacity of Mn_3O_4 nanorod electrode (Fig. 6b) decreased with the increase of the cycle numbers. After 100 cycles, the capacity decreased to 108 mAh/g, which is higher than that of the Mn_2O_3 nanorods electrode. Therefore, the cyclability of both the Mn_2O_3 and Mn_3O_4 electrodes needs to be further improved.

4. Conclusions

In summary, the single-crystalline $MnCO_3$ nanorods were prepared for the first time by a facile hydrothermal method, and the Mn_2O_3 and Mn_3O_4 nanorods were obtained by decomposing the $MnCO_3$ nanorods precursor in air and nitrogen atmosphere,

respectively. The obtained Mn_2O_3 and Mn_3O_4 nanorods can retain the single-crystalline nature of the $MnCO_3$ nanorods and the corresponding growth directions for the $MnCO_3$, Mn_2O_3 and Mn_3O_4 nanorods are [2 1 4], [1 0 0] and [1 1 2], respectively. In the first cycles, the Mn_2O_3 and Mn_3O_4 nanorods as anodes in lithium ion batteries exhibited a lithium storage capacity as high as 998 and 1050 mAh/g, respectively.

Acknowledgements

The authors are grateful for financial support from the Natural Science Foundation of Jiangsu Province (no. BK2009196) and the National Natural Science Foundation of China (no. 51072071)

References

[1] W.Q. Han, S.S. Fan, Q.Q. Li, Y.D. Hu, Science 277 (1997) 1287–1289.
[2] N.R.B. Coleman, M.A. Morris, T.R. Spalding, J.D. Holmes, J. Am. Chem. Soc. 123 (2001) 187–188.
[3] A.M. Morales, C.M. Lieber, Science 279 (1998) 208–211.
[4] Y.N. Xia, P.D. Yang, Y.G. Sun, Y.Y. Wu, B. Mayers, B. Gates, Y.D. Yin, F. Kim, Y.Q. Yan, Adv. Mater. 15 (2003) 353–389.
[5] A.J. Mieszawska, R. Jalilian, G.U. Sumanasekera, F.P. Zamborini, Small 3 (2007) 722–756.
[6] J.G. Lu, P.C. Chang, Z.Y. Fan, Mater. Sci. Eng.: R 52 (2006) 49–91.
[7] J.Y. Chen, B.J. Wiley, Y.N. Xia, Langmuir 23 (2007) 4120–4129.
[8] H. Einaga, S. Futamura, J. Catal. 227 (2004) 304–312.
[9] Y. Lvov, B. Munge, O. Giraldo, I. Ichinose, S.L. Suib, J.F. Rusling, Langmuir 16 (2000) 8850–8857.
[10] J.M. Tarascon, M. Armand, Nature 414 (2001) 359–367.
[11] O. Giraldo, S.L. Brock, W.S. Willis, M. Marquez, S.L. Suib, S. Ching, J. Am. Chem. Soc. 122 (2000) 9330–9331.
[12] Y.F. Shen, R.P. Zerger, R.N. Deguzman, S.L. Suib, L. Mccurdy, D.I. Potter, C.L. O'Young, Science 260 (1993) 511–515.
[13] M. Baldi, S.V. Escribano, J.M.A. Gallardo, F. Milella, G. Busca, Appl. Catal. B 17 (1998) L175–L182.
[14] T. Yamashita, A. Vannice, Appl. Catal. B 13 (1997) 141–155.
[15] V.V. Pankov, Ceram. Int. 14 (1988) 87–91.
[16] A. Vázquez-Olmos, R. Redón, G. Rodríguez-Gattorno, M.E. Mata-Zamora, F. Morales-Leal, A.L. Fernández-Osorio, J.M. Saniger, J. Colloid Interface Sci. 291 (2005) 175–180.
[17] N. Sakai, Y. Ebina, K. Takada, T. Sasaki, J. Electrochem. Soc. 152 (2005) E384–E389.
[18] M. Salavati-Niasari, F. Davar, M. Mazaheri, Polyhedron 27 (2008) 3467–3471.
[19] Y.F. Han, L.W. Chen, K. Ramesh, Z.Y. Zhong, F.X. Chen, J.H. Chin, H.G. Mook, Catal. Today 131 (2008) 35–41.
[20] L.X. Yang, Y.J. Zhu, H. Tong, W.W. Wang, Ultrason. Sonochem. 14 (2007) 259–265.
[21] Z.H. Yang, W.X. Zhang, Q. Wang, X.M. Song, Y.T. Qian, Chem. Phys. Lett. 418 (2006) 46–49.
[22] W.Z. Wang, L. Ao, Cryst. Growth. Des. 8 (2008) 358–362.
[23] K. Ramesh, L.W. Chen, X.Z. Feng, Z.Y. zhong, J.H. Chin, H.W. Mook, Y.F. Han, Catal. Commun. 8 (2007) 1421–1426.
[24] T. Nakamura, A. Kajiyama, Solid State Ionics 124 (1999) 45–52.
[25] M. Tabuchi, K. Ado, H. Kobayashi, H. Kageyama, J. Electrochem. Soc. 145 (1998) L49–L52.
[26] L. Sánchez, J. Farcy, J. Mater. Chem. 6 (1996) 37–39.
[27] S.T. Myung, S. Komaba, N. Kumagai, Electrochem. Acta 47 (2002) 3287–3295.
[28] Z.J. Gu, H.Q. Li, T.Y. Zhai, W.S. Yang, Y.Y. Xia, Y. Ma, J.N. Yao, J. Solid State Chem. 180 (2007) 98–105.
[29] Z.J. Gu, T.Y. Zhai, B.F. Gao, X.H. Sheng, Y.B. Wang, H.B. Fu, Y. Ma, J.N. Yao, J. Phys. Chem. B 110 (2006) 23829–23836.
[30] W.M. Shaheen, M.M. Selim, J. Therm. Anal. Calorim. 59 (2000) 961–970.
[31] H.J. Guo, H.X. Li, Z.X. Wang, W.J. Peng, X. Cao, H.F. Li, J. Power Sources 189 (2009) 95–100.
[32] X.P. Fang, X. Lu, X.W. Guo, Y. Mao, Y.S. Hu, J.Z. Wang, Z.X. Wang, F. Wu, H.K. Liu, L.Q. Chen, Electrochem. Commun. 12 (2010) 1520–1523.